

ene chloride) interact far too strongly with the ion. Experiments to obtain the spectrum of C_{60}^+ using the argon van der Waals complex, $C_{60}Ar^+$, are currently under way, but it is quite possible that even argon is too strong a perturbation. It may be a while yet before the full story is known.

REFERENCES AND NOTES

1. E. A. Rohlfing, D. M. Cox, A. Kaldor, *J. Chem. Phys.* **81**, 3322 (1984). See also D. M. Cox, K. C. Reichman, A. Kaldor, *ibid.* **88**, 1588 (1988) for a more recent review of the carbon cluster literature, together with some new measurements and possible interpretations.
2. J. R. Heath, Q. Zhang, S. C. O'Brien, R. F. Curl, H. W. Kroto, R. E. Smalley, *J. Am. Chem. Soc.* **109**, 359 (1987). Subsequent ultraviolet photoelectron spectral study of these clusters (23) has confirmed that the smaller clusters are linear, those composed of 10 atoms or more prefer at low temperatures the form of a single, monocyclic ring. Entropy effects are expected to favor the opening of such rings at high temperature, forming the long carbon chains observed in the nozzle reactivity experiments and in the interstellar medium.
3. H. W. Kroto, J. R. Heath, S. C. O'Brien, R. F. Curl, R. E. Smalley, *Nature* **318**, 162 (1985).
4. E. Osawa, *Kagaku (Kyoto)* **25**, 854 (1970); Z. Yoshida and E. Osawa, *Aromaticity (Kagakudojin, Kyoto, 1971)*, pp. 174–178.
5. D. A. Bochvar and E. G. Gal'pern, *Dokl. Akad. Nauk SSSR* **209**, 239 (1973); R. A. Davidson, *Theor. Chim. Acta* **58**, 193 (1981); A. D. J. Haymet, *Chem. Phys. Lett.* **122**, 421 (1985).
6. T. G. Schmaltz, W. A. Seitz, D. J. Klein, G. E. Hite, *J. Am. Chem. Soc.* **110**, 1113 (1988).
7. M. D. Newton and R. E. Stanton, *ibid.* **108**, 2469 (1986).
8. Q. L. Zhang *et al.*, *J. Phys. Chem.* **90**, 525 (1986).
9. H. W. Kroto, *Science*, in press.
10. See, for example, A. G. Marshall, *Acc. Chem. Res.* **18**, 316 (1985).
11. J. M. Alford, P. E. Williams, D. J. Trevor, R. E. Smalley, *Int. J. Mass Spectrom. Ion Processes* **72**, 33 (1986).
12. J. L. Elkind, F. D. Wiess, J. M. Alford, R. T. Laaksonen, R. E. Smalley, *J. Chem. Phys.* **88**, 5215 (1988).
13. J. L. Elkind, J. M. Alford, F. D. Wiess, R. T. Laaksonen, R. E. Smalley, *ibid.* **87**, 2397 (1987).
14. S. W. McElvany, H. H. Nelson, A. P. Baronowski, C. H. Watson, J. R. Eyler, *Chem. Phys. Lett.* **134**, 214 (1987).
15. F. D. Weiss, J. L. Elkind, S. C. O'Brien, R. F. Curl, R. E. Smalley, *J. Am. Chem. Soc.* **110**, 4464 (1988).
16. S. C. O'Brien, J. R. Heath, R. F. Curl, R. E. Smalley, *J. Chem. Phys.* **88**, 220 (1988).
17. M. E. Geusic, M. E. Jarrold, T. J. McClrath, R. R. Freeman, W. L. Brown, *ibid.* **86**, 3862 (1986).
18. K. Ragavachari and J. S. Brinkley, *ibid.* **87**, 2191 (1987).
19. A similar change in fragmentation pattern of metastable ions has been observed near C_{30}^+ [P. P. Radi, T. L. Bunn, P. R. Kemper, M. E. Molchan, M. T. Bowers, *ibid.* **88**, 2809 (1988)].
20. The fragment C_2 is a high-energy species, and, even if the cage recloses, roughly 4 eV should be lost per C_2 ejected. Thus when 20 carbon atoms are lost, either a very large number of photons must be absorbed or larger fragments such as C_4 or C_6 must be lost (16).
21. J. R. Heath *et al.*, *J. Am. Chem. Soc.* **107**, 7779 (1985).
22. S. H. Yang, C. L. Pettiette, J. Conceicao, O. Cheshnovsky, R. E. Smalley, *Chem. Phys. Lett.* **139**, 233 (1987).
23. S. Yang *et al.*, *ibid.* **144**, 431 (1988).
24. S. Larsson, A. Volosov, A. Rosen, *ibid.* **137**, 501 (1987).
25. J. R. Heath, R. F. Curl, R. E. Smalley, *J. Chem. Phys.* **87**, 4236 (1987).
26. Carbon cluster research at Rice University has been funded by the National Science Foundation and the Robert A. Welch Foundation. The development of instrumentation was partially funded by the Department of Energy, Division of Chemical Sciences, and the U.S. Army Research Office.

Research Articles

Artificial Airglow Excited by High-Power Radio Waves

P. A. BERNHARDT, L. M. DUNCAN, C. A. TEPLEY

High-power electromagnetic waves beamed into the ionosphere from ground-based transmitters illuminate the night sky with enhanced airglow. The recent development of a new intensified, charge coupled-device imager made it possible to record optical emissions during ionospheric heating. Clouds of enhanced airglow are associated with large-scale plasma density cavities that are generated by the heater beam. Trapping and focusing of electromagnetic waves in these cavities produces accelerated elec-

trons that collisionally excite oxygen atoms, which emit light at visible wavelengths. Convection of plasma across magnetic field lines is the primary source for horizontal motion of the cavities and the airglow enhancements. During ionospheric heating experiments, quasi-cyclic formation, convection, dissipation and reappearance of the cavities comprise a major source of long-term variability in plasma densities during ionospheric heating experiments.

IN 1938, BAILEY PROPOSED THAT A MEGAWATT OF POWER radiated from a ground-based radio transmitter could maintain airglow discharge in the lower ionosphere that would be "about fifty times as bright as the night sky on a moonless night" (1). Although sky brightening of this magnitude has not been achieved, excitation of airglow below the threshold of visual detection, along with a number of other interesting phenomena, has been produced by ionospheric modification by high-power radio waves.

Ionospheric heating experiments require the use of powerful ground-based transmitters to feed a high-gain antenna radiating a

beam of electromagnetic waves into the upper atmosphere. The typical effective radiated power (ERP) in these experiments is 200 MW. The radio wave is partially absorbed near a resonant point where the wave frequency is equal to the plasma frequency. In this interaction region, ordinary mode electromagnetic waves parametri-

P. A. Bernhardt is in the Plasma Physics Division, Naval Research Laboratory, Washington, DC 20375-5000. L. M. Duncan is in the Department of Physics and Astronomy, Clemson University, Clemson, SC 29634. C. A. Tepley is at the Arecibo Observatory, P.O. Box 995, Arecibo, PR 00613.

cally decay into ion-acoustic and plasma waves (2). The plasma is heated by collisional (that is ohmic) processes and by thermalization of energetic electrons driven by electrostatic waves.

The energetic electrons excite neutral atoms that emit light at visible wavelengths. Airglow enhancements at 630.0 nm, the red line of atomic oxygen, were first reported from the Platteville, Colorado, ionospheric modification experiment in 1970 (3). Intensity fluctuations of about 20 rayleighs (1 rayleigh = 10^6 photons $\text{cm}^{-2} \text{s}^{-1}$) were produced by the on-off cycling of 250-MW ERP transmissions of ordinary polarization waves at 5.3 MHz. Subsequent measurements of 630.0-nm airglow enhancements were initially observed at Arecibo, Puerto Rico, in 1972 (4); at Moscow, U.S.S.R., in 1976 (5); and later at Ramfjordmoen near Tromsø, Norway, in 1981 (6). For these observations photometers were employed, each consisting of a narrow-band interference filter, lens, and photomultiplier detector. Spatial scanning and triangulation with the photometers were used to provide rough distributions in intensity and to give emission altitudes (7). The first true images of the artificial airglow were made in 1979 with an all-sky imaging photometer flying in an NKC-135 aircraft near Platteville, Colorado (8). The images showed circular patches with intensities as much as 270 rayleighs above the background. Enhancements of 270 rayleighs (or less) in airglow intensity are far below the visual capability of the human eye, which has a threshold sensitivity of about 20,000 rayleighs at 630.0-nm wavelength.

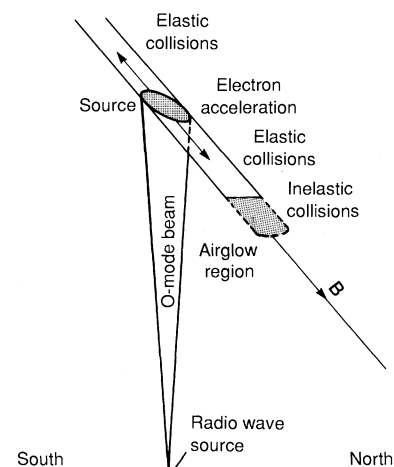
We have recently obtained images of artificial airglow over the Arecibo HF facility. These data have more than a factor of 10 higher spatial resolution than any previously acquired and the images of artificial airglow enhancements show many new physical characteristics of the modified plasma. We find that the airglow clouds are influenced by the earth's magnetic field, by the radiation pattern of the radio beam, by ambient and induced electric fields, and by ionospheric density cavities in the heated volume. The results of the airglow observations complement data taken simultaneously by the Arecibo incoherent scatter radar. The physical processes that couple the optical and radar observations have been studied by means of both experimental and theoretical techniques.

Experiment description and instrumentation. The Arecibo ionospheric heater consists of a high-frequency transmitter connected to a high-gain antenna that radiates vertically. The transmitter was operated at 3.175 MHz up to a power of 400 kW. The electromagnetic wave is emitted from a 4 by 8 inverted log-periodic array with 23-dB gain. The incident power in the F region was, on average, $50 \mu\text{W}/\text{m}^2$.

The primary plasma diagnostic for heating experiments at the Arecibo Observatory in Puerto Rico is the 430-MHz radar. The radar antenna consists of a 305-m fixed reflector and a movable feed that limits the beam pointing to between 0 and 20 degrees of zenith. For azimuth scans, the beam slew rate is 22.50 degrees per minute. During ionospheric modification experiments, plasma densities, drift velocities, electron and ion temperatures, and enhanced plasma lines and ion lines from heater-induced plasma waves and ion-acoustic waves, respectively, can be determined from the incoherent backscatter data. The narrow radar beamwidth (~ 0.1 degree), the restricted range of beam pointing, and the 16 min required to make a 360-degree scan in azimuth limit the usefulness of the radar to mainly line-of-sight observations. Other diagnostic instruments are needed to provide detailed information on the horizontal structure of the modified plasma. One such instrument is a low-light level imager.

We acquired most of the optical data with an intensified charge-coupled device (CCD) camera. The light from the modified region was passed through a 630.0-nm interference filter in front of a 50-mm focal length, $f/0.95$ objective lens. A 40-mm-diameter micro-

Fig. 1. Airglow generation from high-power radio waves. Ordinary-mode electromagnetic radiation is beamed into the ionosphere. At a power above the threshold for the parametric decay instability, large amplitude plasma waves are generated that accelerate ambient electrons. Elastic collisions scatter the electrons in energy and pitch angle. Inelastic collisions absorb energy by excitation of electronic and vibration states of neutral atoms. Radiation from the first excited, metastable state of atomic oxygen yields 630.0-nm (red line) emissions. Electron flux transport among magnetic field lines may displace the airglow region from the energetic electron-source region.



channel plate intensifier provided a luminous gain of 5000 and was externally gated to act as a shutter. A 50-mm, $f/1.2$ relay lens focused the intensified image on a 512 element by 320 element CCD array. The data from each pixel of the CCD array were digitized to 14 bits and stored on magnetic tape. All exposure durations were 30 s. This imaging system has been used for observations of chemical releases in the earth's magnetotail (9) and ionosphere (10).

The digitized images were processed to compensate for nonuniformities in the imaging system and to remove the background airglow. The star images were not suppressed and were used as references for position of the enhanced airglow clouds against the night sky. The absolute intensity of the system was calibrated with a carbon-14 phosphor standard source. The intensity was also checked with data from a 630.0-nm photometer operated with the imager at the Arecibo Airglow Facility.

Theory of enhanced airglow. Artificial airglow is generated by a complex process, which consists of wave-particle interactions, energetic flux transport, collisional excitation and de-excitation, and radiation. The enhanced airglow emissions result from energetic electrons that collisionally excite neutral species in the upper atmosphere (Fig. 1). The source of these electrons could be (i) the tail of a Maxwellian distribution (11) or, more likely, (ii) an electron distribution modified by plasma waves to yield superthermal populations in the heated region (12). The magnitude of the effect depends on the amplitude and the polarization of the electromagnetic pump wave. The threshold field strength for the generation of plasma waves by ordinary mode (O-mode) electromagnetic pump waves is typically about 0.1 V/m (2). In the center of the Arecibo heater beam the field strength exceeds this threshold.

The extraordinary mode (X-mode) polarization wave collisionally heats the plasma without parametric excitation of electrostatic waves (2). X-mode heating temporarily suppresses airglow intensity by reducing the rate of the ambient dissociative recombination reaction

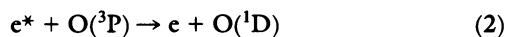


where O^* is an excited state of oxygen that subsequently radiates in a red emission line (630.0 nm) or a green emission line (557.7 nm). This suppression of the natural airglow is usually masked by collisional excitation during O-mode heating.

High-power, O-mode waves are required for enhanced airglow. The strong electromagnetic pump wave from the transmitter excites high-frequency plasma waves near the resonant region where the O-mode reflects. Electrons are accelerated by the electric potential

associated with the plasma waves. Cyclotron acceleration of the electrons becomes important when the parametrically excited plasma waves are near the second harmonic of the electron gyrofrequency and has been used to explain very large airglow enhancements reported at Platteville, Colorado (7). All of the airglow enhancements that we report here were excited by 3.175-MHz O-mode waves that are not near a gyro-harmonic. (The electron gyrofrequency over Arecibo is about 0.98 MHz.)

The measured 630.0-nm emissions come from the O(¹D) state of atomic oxygen. This state is formed by inelastic collisions with electrons having energies above 2 eV. The excitation and radiation reactions are

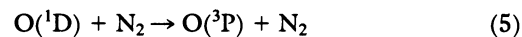


where e^* is an electron with kinetic energy of at least 2 eV, O(³P) is the ground state of atomic oxygen, and $h\nu$ represents a photon with a wavelength of 630.0 nm.

The process is complicated by the presence of molecular nitrogen in the upper atmosphere. Electrons with energies between 2 and 3.5 eV interact with N₂ to produce vibrational states. Consequently, the reaction



acts to absorb energy that could otherwise excite airglow. Also, N₂ can collisionally quench the O(¹D) state by the reaction



In both cases, nitrogen reduces the intensity of the 630.0-nm emissions (11, 13).

The spatial distribution of the airglow is influenced by transport along magnetic field lines. Electrons accelerated out of a localized region may travel to lower altitudes to undergo inelastic collisions in the denser neutral atmosphere (Fig. 1). If this occurs, ground-based observers will record airglow enhancements displaced magnetically to the north of the electron energization region. Elastic collisions with ions and neutrals will impede the flow of field-aligned electron

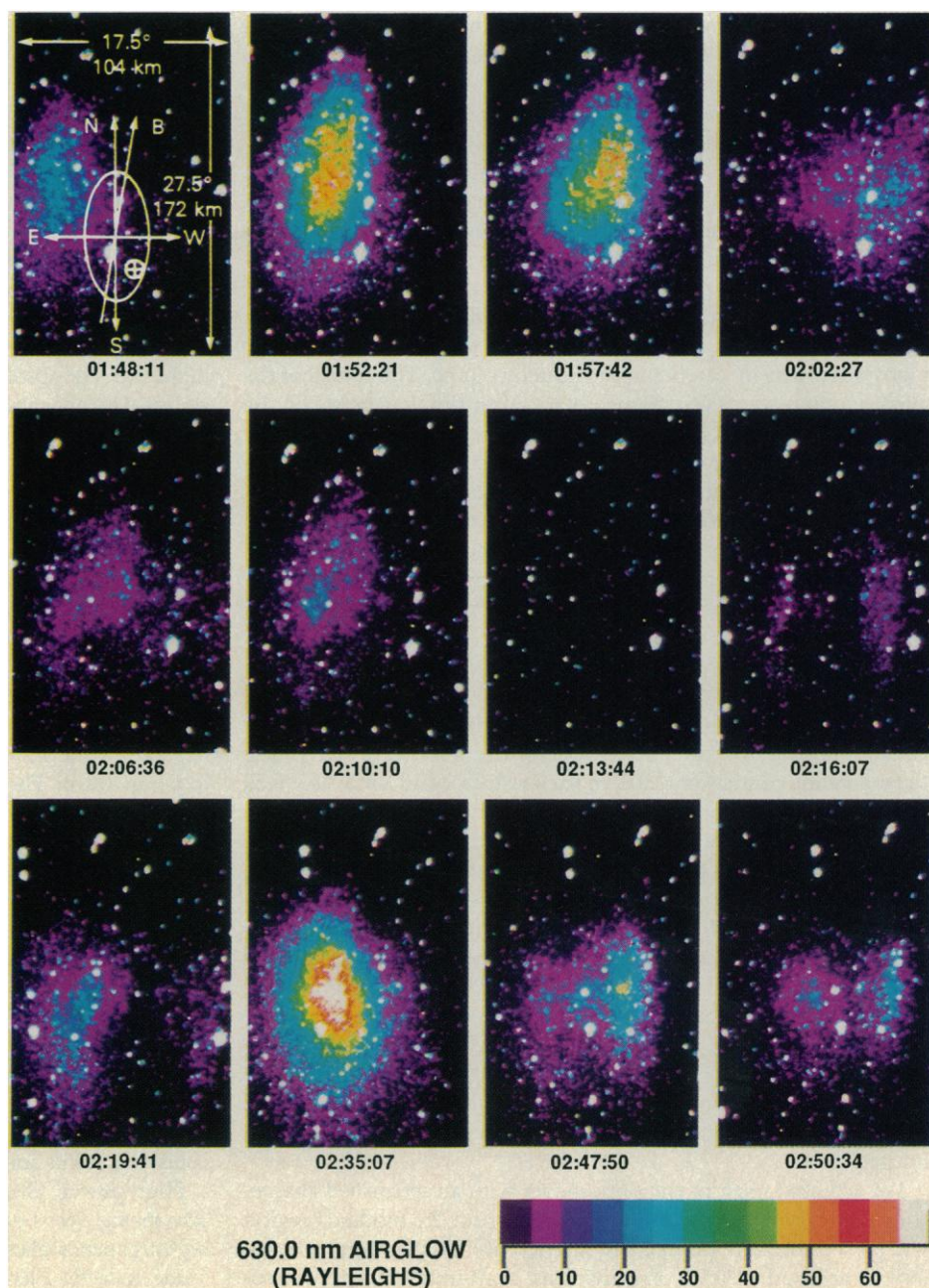


Fig. 2. Airglow clouds over Arecibo in a drifting plasma during ionospheric heating at 3.175 MHz. The motion of three clouds is shown by the three rows of images, respectively. All times are in Atlantic Standard Time (AST) on 3 February 1987. The transmitter is operated at 300 kW to produce the airglow shown in the top row; the clouds drift westward at 58 m/s. The transmitter power is (i) reduced to 150 kW for the first two images of the middle row; (ii) reduced to zero at 02:10:00 AST resulting in the absence of airglow in the third image of the middle row; and (iii) raised to 300 kW at 02:15:00 AST reilluminating the airglow cloud and the associated density cavity. The measured drift velocity for the second cloud is 70 m/s, westward. The third airglow cloud shown in the bottom row drifts westward at 50 m/s.

fluxes. Also, energetic electrons lose energy by elastic collisions with thermal electrons (14).

The intensity pattern of the airglow is also influenced by diffusion of the excited state. The radiative lifetime (τ) of $O(^1D)$ is 148 s, but collisional quenching typically reduces the measured lifetime (11) to between 30 and 100 s. The diffusion coefficient (D) at an altitude of 300 km is about 4×10^{10} cm²/s. Consequently, the scale for diffusive spreading of the cloud ($D\tau$)^{1/2} is of the order of 10 km (11).

By combining theories of (i) energetic electron transport, (ii) excited-state chemistry, and (iii) neutral diffusion, a numerical model can be constructed that relates the airglow intensities to energetic electrons at the source regions. Here, we limit the discussion to the transport of the airglow clouds.

Convection of the airglow enhancements. The motion of artificial airglow clouds was discovered during the January 1986 heating campaign at Arecibo (15) and was studied in greater detail during the January and February 1987 campaigns. When the high-frequency (HF) transmissions were started, an airglow cloud would form in the shape of the antenna radiation pattern. The cloud would usually convect and vanish, only to reappear at the zenith of the heating facility. The cloud velocity was 80 m/s or less. The transport and “snapback” cycle would repeat until the radio beam was turned off.

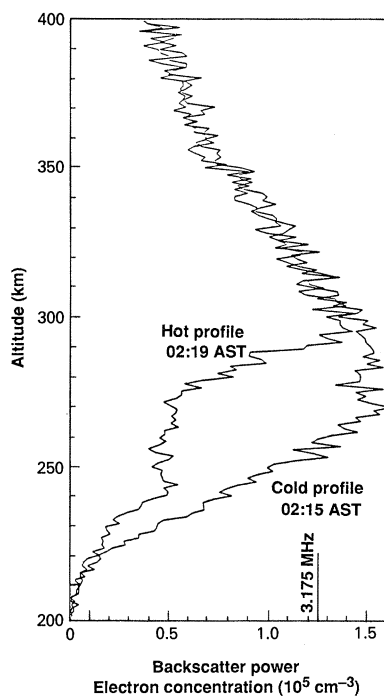
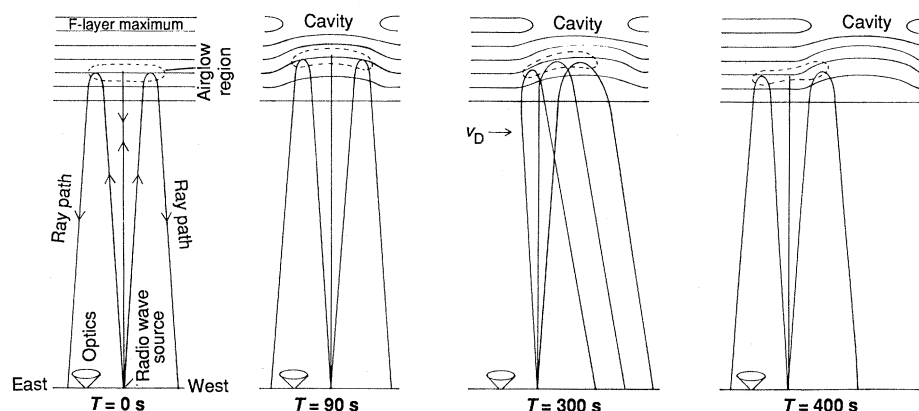


Fig. 3. Comparison of ionospheric profiles for times when the ionospheric heater is off (02:15 AST) and on (02:19 AST). The small amplitude fluctuations are measurement noise. The location of the large bottomside cavity corresponds to the position of the airglow cloud at 02:19:41 (Fig. 2). Variations in the hot profiles can result from horizontal convection of ionospheric cavities.

Fig. 4. Generation of cavity and airglow cloud displacements by continuous-wave heating of a horizontally drifting ionosphere. The HF transmitter excites an airglow enhancement (dashed line) and a thermally driven density cavity (solid-line contours) in the F layer between $T = 0$ and $T = 90$ s. By 300 s after initiation of heating, the cavity and the heater beam are displaced in the direction of the plasma drift. The plasma density gradients on the edge of the cavity refract the ray trajectories of the beam. As the displacement of the beam increases, the effectiveness of the heating is reduced, and the gradients at the edge of the cavity are no longer strong enough to hold the heater beam. By 400 s, the beam moves back to its original position to form another cavity, and the cycle repeats.



We have produced color-coded images of the measured airglow according to intensity in rayleighs (Fig. 2). The background stars and regions of the cloud brighter than 65 rayleighs are shown in white. In the first frame, the 10° by 5° elliptical radiation pattern at 3.175 MHz is shown relative to each airglow panel. The long axis of the ground-based antenna array is oriented east-west so the long axis of the beam pattern is geographically north-south. The zenith of the optical instrument is offset because the HF facility is 17 km north-east of the Arecibo Observatory. Each frame in the series of images covers 104 km by 172 km of the sky at an altitude of 330 km.

The first airglow cloud was generated by a continuous-wave signal with 300 kW transmitter power (Fig. 2, first row). The cloud drifted westward at 54.4 m/s between 01:48 and 02:03 Atlantic Standard Time (AST). The snapback occurred at 02:04 AST and a new cloud was formed at 02:06:36. The influence of the magnetic field is shown by the orientation of the cloud along the direction of B at 01:52:21.

Radar measurements obtained during the same time showed that large-scale cavities were created in the bottomside F layer. Comparison of representative modified and unmodified profiles (Fig. 3) indicates that the absorption of electromagnetic waves in the ionosphere has produced a plasma density reduction. Care, however, must be used in interpreting the backscatter power as purely an electron density reduction because the radar cross section is also reduced with increased electron-to-ion temperature ratios (T_e/T_i). Both electron density depressions and electron temperature enhancements are shown by the backscatter data. We estimate that T_e/T_i is 3 to 4 and the maximum density reduction is 40 percent.

We have developed a phenomenological model for the imager and radar observations (Fig. 4). The unperturbed F layer is horizontally stratified, primarily composed of electrons and O^+ ions. The high-power electromagnetic waves reflect in the ionosphere near the zenith of the transmitter facility. Ohmic heating increases the electron temperature and, consequently, the plasma pressure in the modified ionosphere. A cavity is carved out of the bottomside ionosphere by pressure-induced transport along magnetic field lines. The distorted contour lines at $T = 90$ s represent this cavity. Plasma that is pushed down field lines reacts with neutral molecules to yield polyatomic ions that are subsequently lost by dissociative recombination. Consequently, the integrated number density along a heated field line is reduced. Self-focusing of the electromagnetic wave occurs in the regions of reduced electron concentrations.

At night, the F region may polarize locally by neutral winds blowing across the magnetic field lines. The resulting ambient electric field causes the plasma to drift in the same direction as the wind velocity. During winter, the nocturnal, neutral wind velocity over Arecibo is primarily eastward with velocities from 0 to 120 m/s. The plasma drift velocities tend to be eastward before midnight. The

transition to westward velocities usually occurs around 02:00 local time. This reversal of plasma drifts is due to the influence of polarization fields that map along the earth's magnetic field lines from the conjugate, sunlit F layer (16).

The plasma cavity in the bottom of the ionosphere drifts in response to the external, naturally occurring fields as illustrated by the westward transport of the distorted contour lines between $T = 90$ s and $T = 300$ s (Fig. 4). The dashed airglow region has followed the cavity during this time.

The ray paths of the electromagnetic wave are refracted by the plasma density gradients in the cavity. The ray trajectories are deflected as the density cavity convects away from the zenith of the high-power facility. The effectiveness of the HF beam is reduced by being bent off the sides of the drifting cavity. At $T = 400$ s, the beam cannot be further deflected by the cavity, the electromagnetic wave snaps back to the zenith to form a new cavity (Fig. 4).

During the 1987 heating campaigns, the incoherent-scatter radar and the Fabry-Perot interferometer were used to provide independent measurements of plasma drifts and neutral winds, respectively. The artificial airglow clouds were found to be moving in the direction of the plasma drift, sometimes with a velocity that exceeded ion velocity.

During the observations near midnight, the measured neutral wind speed was 60 m/s in the eastward direction. The measured plasma drift velocity during the same period of time on 28, 29, and 30 January 1987 was 30 to 40 m/s westward. Consequently, the relative velocity between the neutrals and the plasma was 90 to 100 m/s. As stated earlier, the first cavity (Fig. 2) moved westward at a velocity of more than 50 m/s. During this period of time, the cavities and associated airglow were transported in opposition to the neutrals with velocities that were 10 to 20 m/s larger than that of the ambient plasma.

To test if the heater power had an influence on the motion of the airglow cloud, we reduced the heater power by 50 percent to 150 kW at 02:05 AST. This accounts for the weaker airglow in the frames at 02:06:36 and 02:10:10 (Fig. 2). At 02:10:00, the heater power was reduced to zero, and any preexisting cavity was allowed to drift unheated for 5 min. When the HF power was returned to 300 kW at 02:15:00, the airglow reappeared at a location consistent with a westward convection velocity of 70 m/s. The speed of the plasma cavities increased when the heater was off. The image at 02:16:07 (Fig. 2) shows two airglow clouds; the one on the right outlines the old cavity and the one on the left indicates the formation of a new cavity. The HF beam was split in two by the density structure in the ionosphere.

The third airglow cloud appeared to the west of the heater and remained stationary for about 15 min (Fig. 2, last four panels). At 02:35:07, this cloud seemed to have been caught by the plasma drift and was transported westward at 50 m/s.

The position of the airglow clouds between 01:30 and 03:00 AST varied by over 60 km (Fig. 5). The northward and westward displacements of the bright part of each cloud are plotted relative to the zenith of the ionospheric heating facility. Four snapbacks occurred at 01:45, 02:03, 02:17, and 02:53 AST. The east-west displacements were confined to ± 32 km of the heater.

The apparent motion of the cavity was modified by the HF transmissions. When the heater was on, the westward velocity of the cavity was between 50 and 55 m/s. The cavity velocity increased to 70 m/s when the heater was turned off for 5 min (Fig. 5).

The northward displacement of the cloud was limited to 10 to 25 km (Fig. 5, top graph). The northward displacements are less accurately determined than the westward displacements because of the meridional elongation of the heater beam. But the airglow clouds always stay to the north of the heater.

Theory of drifting cavities. The optical observations indicate that plasma-density cavities produced by ionospheric heating experiments can move at velocities larger than the plasma drift velocity when there is a large neutral wind in opposition to the ambient plasma motion. The additional velocity of the cavities comes from electric fields internally generated by polarization of the plasma. In the F region, where the ion collision frequency is much less than the ion gyrofrequency, a neutral wind (U) perpendicular to the magnet-

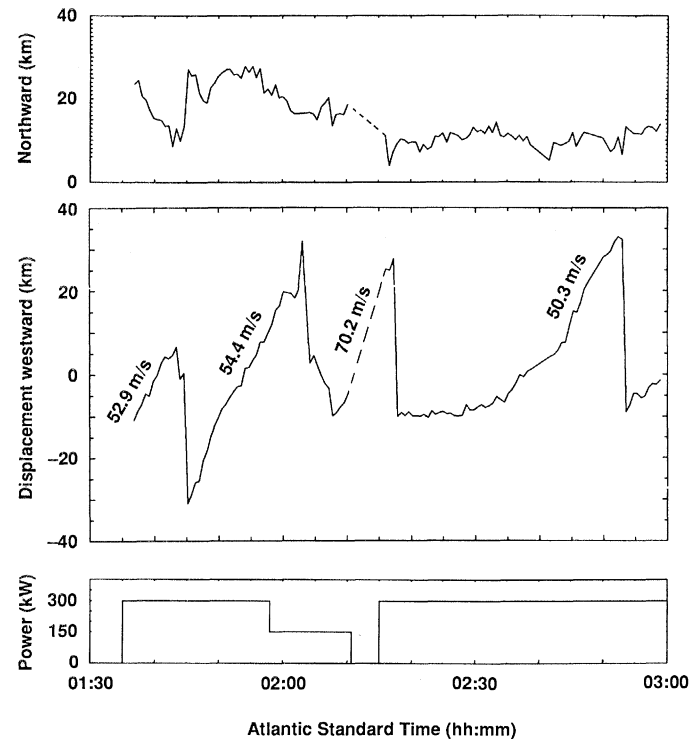


Fig. 5. Location of airglow clouds on 3 February 1987 relative to the zenith of the ionospheric heater. The slopes of the displacement versus time curves are used to obtain the drift speeds. The heater power is reduced to zero between 02:10 and 02:15 AST. The induced cavity drifts significantly faster during this "off" period. The snapbacks occur for displacements of about 32 km in the westward direction.

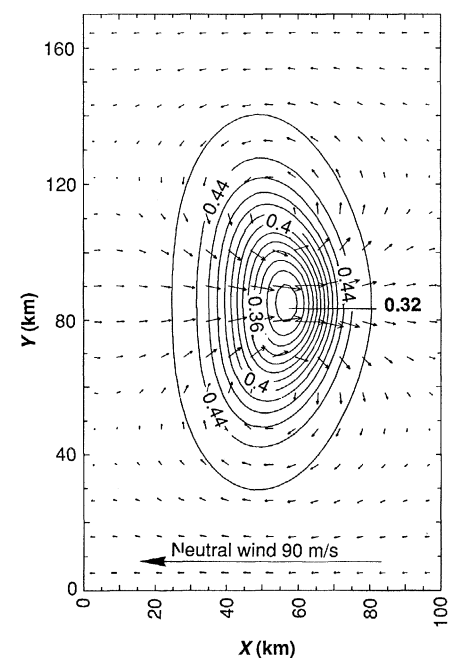


Fig. 6. Numerical calculations of induced drifts (small arrows) in a plasma density cavity at $T = 642.7$ s. The contours of a 30 percent depletion of integrated Pedersen conductivity (in mhos) become distorted by internally generated polarization electric fields. A 90 m/s neutral wind blowing from right to left (negative x direction) induces the flow indicated by the arrows. The maximum induced velocity is 10 m/s in the positive x direction.

ic field (\mathbf{B}) will produce a Hall drift of the ions in the $\mathbf{U} \times \mathbf{B}$ direction (17). (Here \mathbf{U} is the neutral velocity in the rest frame of the plasma.) The resulting charge separation in the cavity yields a polarization electric field \mathbf{E} that will oppose $\mathbf{U} \times \mathbf{B}$. This field causes the electrons and ions to drift against the neutral wind.

The motion of artificially created plasma cavities is modeled by means of a two-dimensional transport code (18). The electric potential inside the cavity is found from the following dynamo equation

$$\Delta \cdot [\Sigma_p \Delta \phi] = (\mathbf{U} \times \mathbf{B}) \cdot \nabla \Sigma_p \quad (6)$$

where Σ_p is the field line-integrated Pedersen conductivity and ϕ is the electric potential. The plasma drift velocity is found from

$$\mathbf{U} = \mathbf{E} \times \mathbf{B} / B^2 \quad (7)$$

where $\mathbf{E} = -\nabla \phi$ is the electric field. The ion concentration is given by the continuity equation

$$\frac{\partial n}{\partial t} + \Delta \cdot (n\mathbf{v}) = 0 \quad (8)$$

where n is the ion number density.

The plasma density couples to the potential equation through the Pedersen conductivity

$$\Sigma_p = \int \frac{e\nu}{B\Omega} n ds \quad (9)$$

where ν is the ion-neutral collision frequency, Ω is the ion gyrofrequency, e the electron charge, and ds the incremental distance along the magnetic field line.

The horizontal motion of a representative cavity is calculated with the computer code. The unperturbed field line-integrated Pedersen conductivity is $\Sigma_{p0} = 0.46$ mho. The simulation was initialized with an elliptically shaped cavity of the form

$$\Sigma_p(x, y) = \Sigma_{p0} \left[1 - 0.3 \exp \left(-\frac{x^2}{2\sigma_x^2} - \frac{y^2}{2\sigma_y^2} \right) \right] \quad (10)$$

where $\sigma_x = 10$ km and $\sigma_y = 20$ km and the coordinates x and y correspond to the west and north directions, respectively, in the images (Fig. 2). This cavity model is consistent with the 3 February 1987 radar and optical measurements. The plasma is in the rest frame of the computation. The neutral wind velocity is 90 m/s in the negative x direction.

The results of the simulation (Fig. 6) show contours of integrated Pedersen conductivity drawn on top of the plasma velocity flow field. Near the center of the cavity, the drift velocity is increased by 10 m/s. From the spacing of the contours, it is apparent that the nonuniform flow steepens the plasma gradient on the right side of the cavity. Similar steepening is seen in some of the optical data.

Summary and conclusions. The airglow images show several previously unreported phenomena including: (i) geomagnetic field alignment, (ii) drift-snapback cycle, including fixed limit to maximum displacement at snapback, (iii) superplasma drift velocities that are larger when the heater is off, and (iv) northward displacement of the airglow clouds. The motion of the airglow enhancements provides explanations for two previously observed phenomena at Arecibo. First, a major source of the long-term variability in the ionospheric modification phenomenology (19) has been established to be drifting density cavities. Second, the temporal variations in the

630.0-nm intensity measured by fixed position photometers (20) are explained by drifting airglow clouds. The movement of airglow clouds across the photometer field-of-view causes these apparent intensity fluctuations.

The slowing down of the drifting cavity when the heater is on may result from (i) shorting out of electric fields in the high-temperature plasma or (ii) erosion of the side of the cavity by the beam. The stagnation of the airglow clouds between 02:18 and 02:33 suggests that the beam, at times, may be strong enough to reform the cavity faster than it can be transported away from the zenith of the heating facility. We are extending our numerical models of ionospheric heating (21) to investigate this behavior.

It has been suggested that the airglow transport may be caused by traveling ionospheric disturbances (TIDs) produced by acoustic gravity wave in the upper atmosphere (22). We believe that the drifting cavities are responsible for the long-term convection and that TIDs will introduce transient perturbations into the motion of the airglow clouds.

More research is needed to determine the relationship between the airglow clouds, the density cavities, and the electron accelerations. Analysis of data acquired at Arecibo during coordinated radar and optical observations may clarify these relationships. Future models will allow us to trace the complete wave-wave interaction process from radiation of EM waves at ground level to the generation of electrostatic waves in the ionosphere to radiation of visible waves out of the upper atmosphere.

REFERENCES AND NOTES

1. V. A. Bailey, *Phil. Mag.* **26**, 425 (1938).
2. J. A. Fejer, *Rev. Geophys. Space Phys.* **17**, 135 (1979).
3. W. F. Utlaug and R. Cohen, *Science* **174**, 245 (1971).
4. W. E. Gordon and H. C. Carlson, Jr., *Radio Sci.* **9**, 1041 (1974).
5. T. G. Adeishvili *et al.*, *Sov. J. Plasma Phys.* **4**, 721 (1978).
6. P. Stubbe *et al.*, *J. Atm. Terr. Phys.* **44**, 1025 (1982). Repeated attempts to detect heater-induced airglow at high latitudes has failed, possibly due to the masking effects of the natural aurora.
7. J. C. Haslett and L. R. Megill, *Radio Sci.* **9**, 1005 (1974).
8. J. G. Moore, *Environmental Research Paper No. 852*, AFGL-TR-83-0238 (Air Force Geophysics Laboratory, Bedford, MA, 1983).
9. P. A. Bernhardt *et al.*, *J. Geophys. Res.* **92**, 5777 (1987).
10. P. A. Bernhardt, B. A. Kashiwa, C. A. Tepley, S. T. Noble, *Astrophys. Lett. Comm.* **27**, 169 (1988).
11. D. P. Sipler and M. A. Biondi, *J. Geophys. Res.* **77**, 6202 (1972); D. P. Sipler, E. Enemark, M. A. Biondi, *ibid.* **79**, 4276 (1974).
12. J. A. Fejer and K. N. Graham, *Radio Sci.* **9**, 1081 (1974); J. Weinstock, *J. Geophys. Res.* **80**, 4331 (1975).
13. H. C. Carlson, V. B. Wickwar, G. P. Mantas, *J. Atm. Terr. Phys.* **44**, 1089 (1982).
14. P. M. Banks, C. R. Chappell, A. F. Nagy, *J. Geophys. Res.* **79**, 1459 (1974).
15. P. A. Bernhardt, L. M. Duncan, C. A. Tepley, R. A. Behnke, J. P. Sheerin, *Adv. Space Res.* **8**, 271 (1988).
16. R. G. Burnside, J. C. G. Walker, R. A. Behnke, C. A. Gonzales, *J. Geophys. Res.* **88**, 6259 (1983).
17. H. Rishbeth and O. K. Garriott, *Introduction to Ionospheric Physics* (Academic Press, New York, 1969).
18. P. A. Bernhardt, *J. Geophys. Res.* **93**, 8696 (1988).
19. L. M. Duncan and E. A. Behnke, *Phys. Rev. Lett.* **41**, 998 (1978); F. T. Djuth, B. Thide, H. M. Ierkic, M. P. Sulzer, *Geophys. Res. Lett.* **14**, 953 (1987); L. M. Duncan, J. P. Sheerin, R. A. Behnke, *Phys. Rev. Lett.* **61**, 239 (1988).
20. J. A. Fejer, *J. Atmos. Terr. Phys.* **47**, 1165 (1985).
21. P. A. Bernhardt and L. M. Duncan, *ibid.* **44**, 1061 (1982); *ibid.* **49**, 1107 (1987).
22. C. O. Hines, *Can. J. Phys.* **38**, 1441 (1960); K. C. Yeh and C. H. Liu, *Rev. Geophys. Space Phys.* **12**, 193 (1974); S. H. Francis, *J. Atm. Terr. Phys.* **37**, 1011 (1975).
23. We acknowledge discussions with F. T. Djuth during the course of this work. The ionospheric heating experiments were started while two of us (P.A.B. and L.M.D.) were at Los Alamos National Laboratory. We thank D. J. Simons of LANL for lending the optical equipment used to acquire the low-light level images, and the Arecibo Observatory staff for their cooperation and assistance. The Arecibo Observatory is operated by Cornell University under contract to the National Science Foundation. Support has come in part from the Office of Naval Research. 19 July 1988; accepted 5 October 1988